Exceptional-Point Stability Boundaries from Quantum Dissipation to Cosmological Acceleration

Nate Christensen

SymC Universe Project, Missouri, USA

`NateChristensen@SymCUniverse.com`

09 February 2026

Abstract

Dissipative dynamics across physical systems exhibit organizing structural boundaries. The dimensionless damping ratio $\chi \equiv \gamma/(2\omega)$ defines a stability architecture in which the critical threshold $\chi = 1$ marks a second-order non-Hermitian Exceptional Point (EP). A parameter-free identity is derived linking cosmic acceleration to critical damping, $\chi_\delta = 1 \iff q = 0$, indicating a structural constraint on the timing of dark energy dominance. The result is structural rather than causal: it follows from the form of the growth and Friedmann equations within flat ΛCDM, independent of any microscopic model for dark energy. This stability condition propagates through a substrate inheritance relation, whereby emergent modes inherit EP structure from vacuum precursors. Within this framework, the observed particle distribution is consistent with stability organization: long-lived matter occupies localized stability basins at $\chi \ll 1$, while short-lived excitations cluster near the $\chi = 1$ interface. The framework replaces ad hoc parameter tuning with a stability-based classification principle.

1 Boundary Structure in Dissipative Dynamics

Many physical theories are structured around boundary conditions and limiting principles. The speed of light c limits information propagation, and Planck's constant $\hbar$ bounds measurement precision. The dimensionless ratio

$$\chi \equiv \frac{\gamma}{2\omega} \tag{1}$$

plays an analogous role in dynamical stability. This stability-boundary formalism is developed in Ref. [24] and identifies $\chi = 1$ as a structural separatrix in dissipative dynamics.

At $\chi = 1$, the generator of dynamics becomes defective and the impulse response transitions to

$$h(t) = te^{-|\omega|t}, \tag{2}$$

defining a second-order non-Hermitian exceptional point (EP2) [1, 11–13].

Quadratic eigenproblems for linear response arise across classical dissipative modes, retarded propagators in open quantum field theory, and cosmological growth dynamics [4, 6, 9, 17]. In each case, the exceptional-point kernel appears when the damping rate matches twice the characteristic frequency, $\chi = \gamma/(2\omega) = 1$. Markovian open-system generators of Lindblad type can realize the

same EP2 structure in suitable reduced response channels or effective mode equations (Supplementary Section 1) [10, 14], but the EP condition is asserted here at the level of the shared quadratic response structure.

For representative linear response channels with Gaussian noise and finite bandwidth, an information-efficiency functional $\eta(\chi) \equiv I(\chi)/\Sigma(\chi)$ admits a strict local maximum in a narrow neighborhood of $\chi = 1$ under standard smoothness conditions (Supplementary Section 2). This supports the interpretation of near-critical damping as a robust operating point balancing responsiveness against dissipation in common model classes.

A strict local maximum at $\chi = 1$ follows if $\eta(\chi)$ is twice differentiable in a neighborhood of $\chi = 1$, $\eta'(1) = 0$, and $\eta''(1) < 0$. The Gaussian-channel examples provide an explicit realization of these conditions.

Most significantly, the onset of cosmic acceleration ($q = 0$) is mathematically identical to the structure growth field reaching critical damping ($\chi_\delta = 1$), providing a structural correspondence for the timing of late-time acceleration without fine-tuning.

2 Exceptional-Point Kernel and Efficiency Extremum

For a representative linear mode whose observable response obeys a second-order dissipative equation:

$$\ddot{x} + \gamma \dot{x} + \omega^2 x = 0, \tag{3}$$

the characteristic discriminant

$$\Delta = \gamma^2 - 4\omega^2 = 4\omega^2(\chi^2 - 1) \tag{4}$$

vanishes at $\chi = 1$, yielding coalesced roots $\lambda_\pm = -|\omega|$ and the EP2 impulse kernel (2) [12]. Such quadratic response structures appear directly in classical linear-response theory and in retarded propagators of dissipative quantum field theory [4]. Lindblad-form Markovian dynamics can realize the same EP2 kernel in appropriate effective response channels; the mapping and its scope are given explicitly in Supplementary Section 1 [10, 14].

An identical structure arises in dissipative quantum field theory. For a scalar mode with retarded propagator

$$G_R(\Omega) = \frac{1}{-\Omega^2 - i\gamma\Omega + \omega^2}, \tag{5}$$

the poles

$$\Omega_\pm = -\frac{i\gamma}{2} \pm \sqrt{\omega^2 - \frac{\gamma^2}{4}} \tag{6}$$

coalesce at $\gamma = 2|\omega|$, reproducing the same EP2 kernel [4, 13].

The information-efficiency functional

$$\eta(\chi) \equiv \frac{I(\chi)}{\Sigma(\chi)} \tag{7}$$

exhibits a strict local maximum at $\chi = 1$ in Gaussian channel models (Supplementary Section 2). This identifies $\chi = 1$ as a recurrent structural boundary in systems that simultaneously admit responsiveness and stability.

Physically, $\chi < 1$ corresponds to persistent ringing, while $\chi > 1$ sacrifices responsiveness. Realistic constraints broaden the optimum to a narrow window near criticality [15]. Figure 1 visualizes this dual structure as an exceptional-point manifold separating overdamped and underdamped regimes.

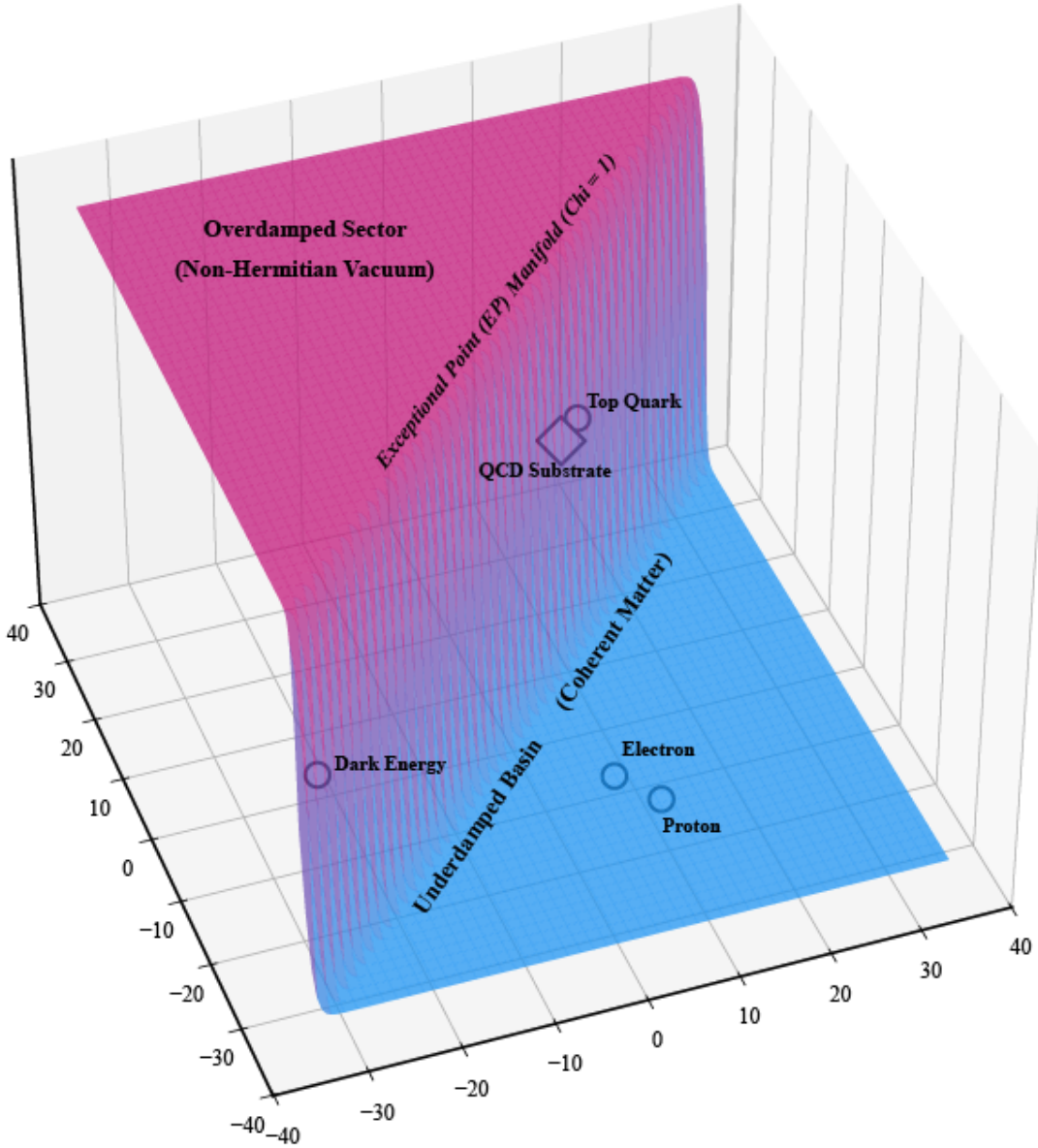**Non-Hermitian Topology of the Vacuum-to-Matter Interface**

Figure 1: **Topological structure of the stability manifold.** Three-dimensional visualization in $(\log_{10} \omega, \log_{10} \Gamma, \chi)$ space where $\chi = \Gamma/(2\omega)$ is the dimensionless damping ratio. The colored surface represents the exceptional point (EP) manifold at $\chi = 1$, separating overdamped ($\chi > 1$, magenta) and underdamped ($\chi < 1$, blue) dynamical regimes. Representative systems illustrate an ordering by observed stability index: vacuum-lineage processes appear near the critical line, while long-lived excitations lie deep in the underdamped basin. The schematic language is classificatory and does not assert a microscopic pathway. Vertical projection lines connect the 3D topology to the empirical validation plane (Figure 3).

Structural interpretation

The exceptional-point boundary at $\chi = 1$ is not interpreted as a dynamical attractor. Rather, it serves as a structural separatrix where impulse response transitions from oscillatory to monotone decay. In representative dissipative channels (second-order systems with Gaussian noise and finite bandwidth), the information-efficiency functional $\eta(\chi)$ admits a strict local maximum at $\chi = 1$. Departures from $\chi \approx 1$ incur complementary penalties: $\chi < 1$ produces persistent ringing that degrades signal fidelity under finite bandwidth, while $\chi > 1$ produces slow relaxation that suppresses information throughput for fixed dissipation. The framework interprets near-critical operation as a robust efficiency extremum, consistent with observed system clustering in the range $0.8 \lesssim \chi \lesssim 1.0$.

3   Cosmic Crossing: $\chi_\delta = 1 \Longleftrightarrow q = 0$

Linear density perturbations satisfy

$$\ddot{\delta} + 2H\dot{\delta} - 4\pi G \rho_m \delta = 0 \tag{8}$$

[9, 17], yielding

$$\chi_\delta = \frac{H}{\sqrt{4\pi G \rho_m}}. \tag{9}$$

In flat ΛCDM, the deceleration parameter

$$q = \frac{1}{2}\Omega_m - \Omega_\Lambda \tag{10}$$

vanishes at $\Omega_m = 2/3$. The Friedmann equations then give

$$H^2 = 4\pi G \rho_m, \tag{11}$$

implying the exact identity

$$\chi_\delta = 1 \Longleftrightarrow q = 0. \tag{12}$$

This parameter-free identity links cosmic acceleration onset to critical damping of structure growth.

Scope of the identity.   Equation (12) holds *exactly* for spatially flat ΛCDM. In non-flat cosmologies or in wCDM with $w \neq -1$, the synchronization between the acceleration transition and the critical-damping crossing is no longer exact, but the stability crossing $\chi_\delta = 1$ remains well-defined and shifts to a nearby redshift. This makes departures from ΛCDM testable as measurable offsets between the $q = 0$ and $\chi_\delta = 1$ transitions. Figure 2 demonstrates this synchronization.
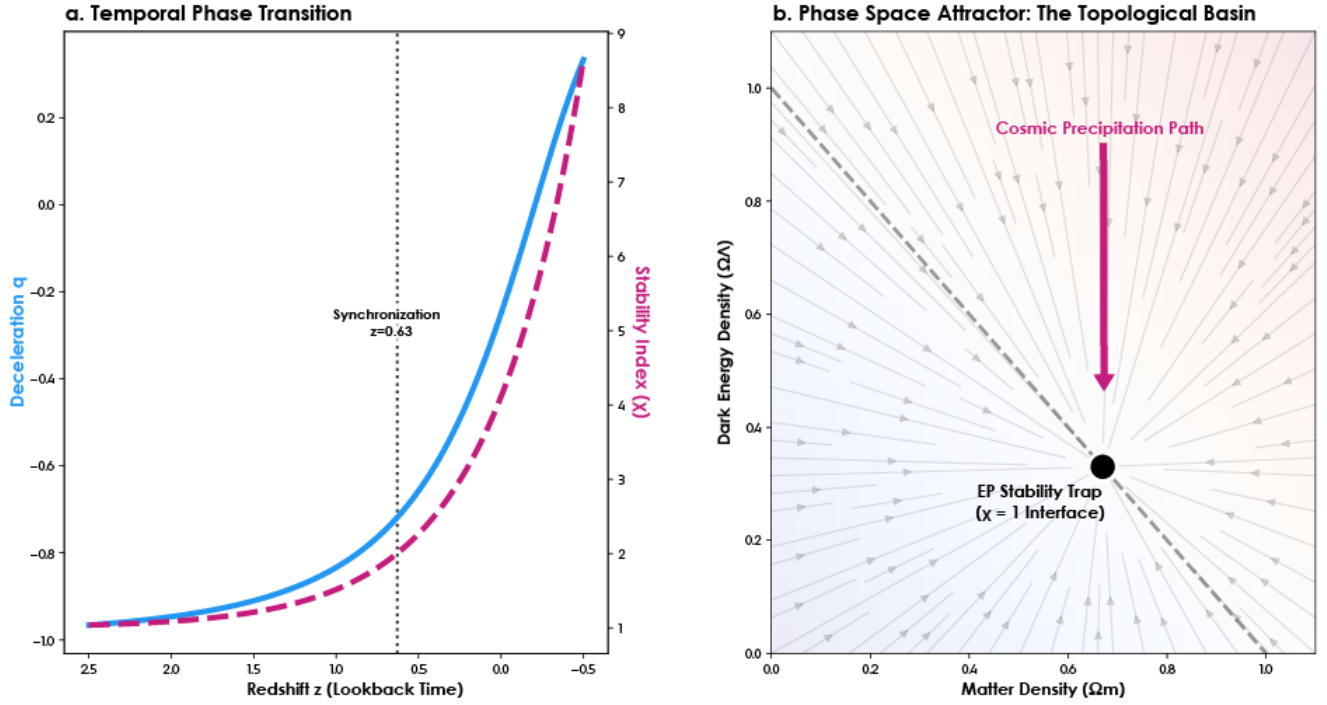
Figure 2: **Cosmological synchronization of critical damping and acceleration onset. (a)** Temporal evolution showing the deceleration parameter $q(z)$ (blue) and stability index $\chi_\delta(z)$ (magenta dashed) as functions of redshift, computed directly from the flat-ΛCDM Friedmann and growth equations with concordance parameters $\Omega_m = 0.315$, $\Omega_\Lambda = 0.685$ [19]; no fitting functions are used. Both curves cross at $z_t \approx 0.63$, where $q = 0$ and $\chi_\delta = 1$ simultaneously. **(b)** Phase-space trajectory in $(\Omega_m, \Omega_\Lambda)$ coordinates under concordance ΛCDM. Flow lines converge toward the critical point $\Omega_m = 2/3$, $\Omega_\Lambda = 1/3$ where the structural identity is satisfied; the star marks the present-day concordance values.

This result is parameter-free within flat ΛCDM and independent of any cosmological origin model [18–20].

4 Robustness Under Interactions and Memory

In weakly interacting $\lambda\phi^4$ theory, renormalization-group flow yields

$$\frac{d\chi}{d\ell} = (a_\gamma - a_\omega)\lambda\chi, \tag{13}$$

so that χ remains marginal when $a_\gamma \approx a_\omega$ [22]. One-loop calculations confirm $|\Delta\chi| < 0.3\%$ over three decades, with two-loop corrections of order 3×10^{-5} (see Supplementary Section 6 for explicit one-loop and two-loop derivations) [23].

Finite-memory baths with kernel $K(t) = \gamma_0 e^{-t/\tau}$ yield an effective damping

$$\gamma_{\text{eff}}(\omega) = \frac{\gamma_0}{1 + (\omega\tau)^2}, \tag{14}$$

broadening but not destroying the critical boundary [4, 7] (see Supplementary Section 10 for fractional and power-law memory extensions). The physically realized damping ratio in such environments is therefore

$$\chi_{\text{phys}}(\omega) \equiv \frac{\gamma_{\text{eff}}(\omega)}{2\omega} = Z(\omega\tau)\,\chi_{\text{bare}}, \qquad Z(\omega\tau) = \frac{1}{1 + (\omega\tau)^2} < 1, \tag{15}$$

so that the exceptional point at $\chi_{\text{bare}} = 1$ corresponds to a downward-shifted operating point when expressed in terms of effective rates.

5 Substrate Inheritance as a Structural Relation

Let $\{\phi_k\}$ denote substrate modes with frequencies Ω_k and damping Γ_k. Any emergent mode $\psi = \sum_k c_k \phi_k$ inherits effective parameters

$$\Omega_\psi^2 = \sum_k |c_k|^2 \Omega_k^2, \qquad \Gamma_\psi = \sum_k |c_k|^2 \Gamma_k. \tag{16}$$

The resulting damping ratio is

$$\chi_\psi = \frac{\Gamma_\psi}{2\sqrt{\Omega_\psi^2}}. \tag{17}$$

To make the overlap structure intrinsic, define the stabilized substrate subspace $\mathcal{H}_s$ and the corresponding orthogonal projector

$$\mathcal{P}_s \equiv \sum_{i \in s} |\phi_i\rangle\langle\phi_i|. \tag{18}$$

For any proto-mode $|\psi_{\text{proto}}\rangle$, the substrate overlap is defined geometrically as

$$\epsilon_\psi \equiv \|\mathcal{P}_s|\psi_{\text{proto}}\rangle\|^2 = \langle\psi_{\text{proto}}|\mathcal{P}_s|\psi_{\text{proto}}\rangle. \tag{19}$$

In a substrate eigenbasis this reduces to $\epsilon_\psi = \sum_{i \in s} |\langle\phi_i|\psi_{\text{proto}}\rangle|^2$. A dimensional illustration of how small overlap coefficients ($\epsilon \ll 1$) naturally generate hierarchically small masses in weak-mixing scenarios is provided in Supplementary Section 5.

Empirically, long-lived particles occupy the underdamped basin $\chi \ll 1$, while short-lived resonances cluster near $\chi \approx 1$. This distribution is shown in Figure 3; the numerical compilation and conventions used in the classification are provided in Supplementary Table S1.
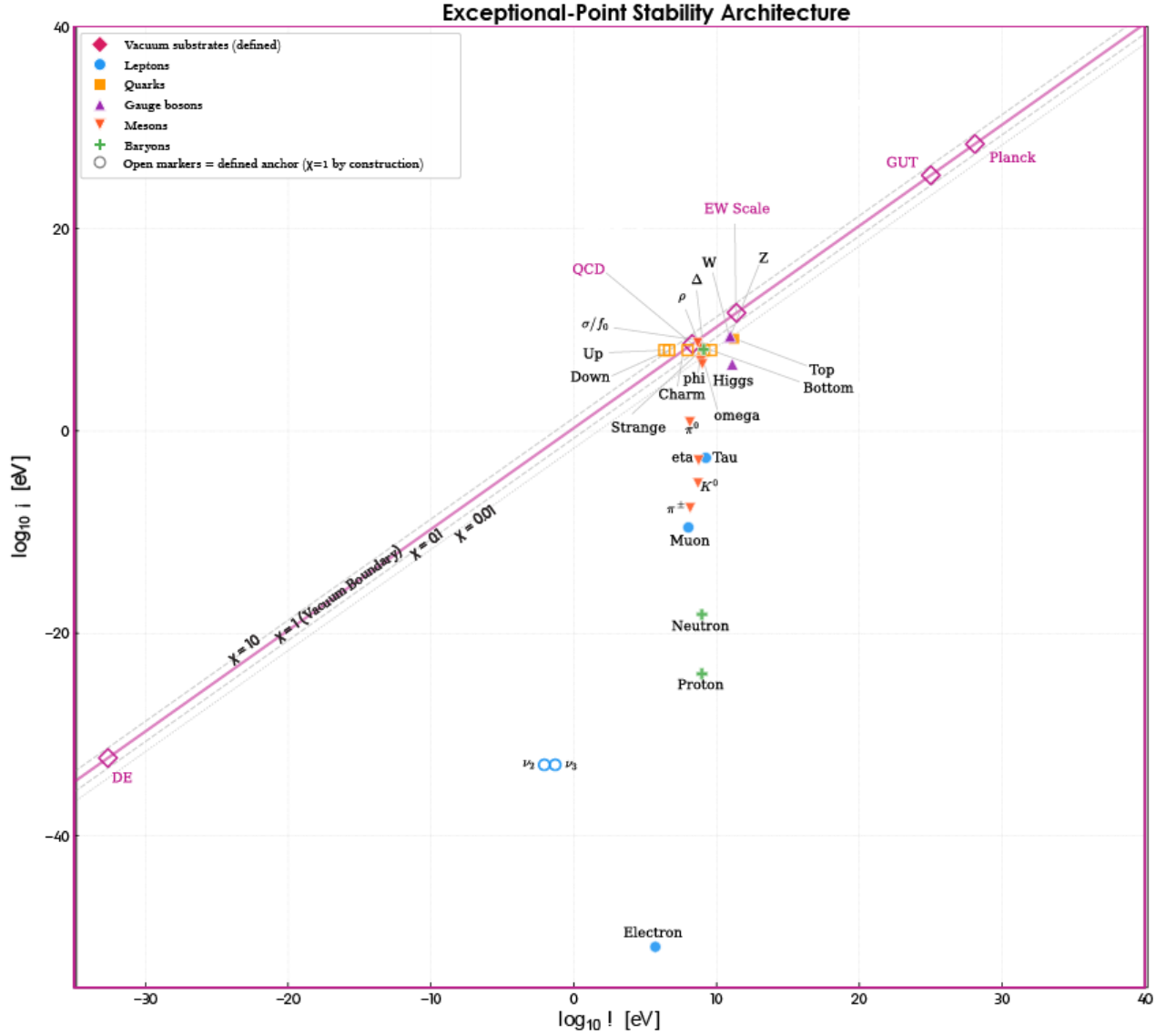
Figure 3: **Exceptional-Point Stability Architecture: cross-scale classification.** Physical systems plotted as damping scale $\log_{10}\Gamma$ versus characteristic frequency $\log_{10}\omega$ from cosmological to Planck scales. The solid magenta line marks the $\chi = \Gamma/(2\omega) = 1$ exceptional-point boundary; dashed lines show constant-χ reference levels at $\chi = 0.01$, 0.1, and 10. For elementary particles, ω is identified with rest mass (natural units) and Γ with the measured decay width [16]. **Open markers** indicate vacuum-substrate anchors defined by the critical-damping condition $\Gamma = 2\omega$ ($\chi = 1$ by construction); these are theoretical reference points, not measured decay widths, and are excluded from statistical estimates. **Filled markers** represent empirical PDG data. Long-lived matter occupies the deep underdamped basin ($\chi \ll 1$, lower left); short-lived resonances and vacuum substrates cluster at the $\chi = 1$ boundary. Exact values and conventions in Supplementary Table S1.

Null-model comparator. For comparison, Monte Carlo null ensembles constructed from independent log-uniform (Ω, Γ) samples over the observed ranges produce substantially broader χ distributions than those shown here. This comparison is intended to illustrate structural contrast rather than to assert formal statistical significance.

When a dominant substrate satisfies $\chi \approx 1$, any emergent mode with nonzero overlap carries

a corresponding near-critical contribution. In the dominance limit, $|c_s|^2 \gg |c_{k \neq s}|^2$, the emergent ratio approaches $\chi_\psi \to \chi_s$. Within the present stability architecture, emergent parameters are defined through projection onto substrate modes, thereby constraining the admissible parameter space relative to arbitrary independent tuning. A formal treatment of this relation is provided in Ref. [24].

5.1 Structural Role of Gauge Couplings

Within the stability architecture, gauge couplings are classified as *substrate-ratio parameters*. In representative open-field settings, interaction-induced broadening rates admit scaling of the form $\Gamma_i \propto g_i^2 \Omega_i$ up to model-dependent phase-space factors and kinematic thresholds, where Ω_i denotes a characteristic sector frequency at the scale of interest. The effective stability index $\chi_i = \Gamma_i/(2\Omega_i)$ therefore depends directly on the gauge coupling.

The persistence of a gauge sector as a coherent substrate is consistent with operation within the near-critical window $\chi_i \approx 1$. This condition constrains g_i^2 to values that maintain spectral balance between interaction-induced damping and coherent propagation across renormalization-group flow. In this sense, gauge couplings can be interpreted as ratios constrained by stability consistency within the present framework, rather than as completely unconstrained free inputs.

The research does not claim a parameter-free derivation of the numerical values of (g_1, g_2, g_3). Instead, it provides a stability-based classification: the couplings control the ratio between interaction-induced broadening and coherent sector frequency, and therefore determine whether a sector admits near-critical operation in the sense of $\chi_i = \Gamma_i/(2\Omega_i)$. Any stronger claim requires specifying (Ω_i, Γ_i) operationally and demonstrating the mapping to the measured renormalized couplings at a fixed reference scale.

6 Experimental and Observational Tests

Having established the structural role of the $\chi = 1$ boundary across quantum, field-theoretic, and cosmological dynamics, this section outlines concrete experimental and observational tests capable of confirming or falsifying the stability architecture.

The structural identity of the $\chi = 1$ boundary yields falsifiable predictions across accessible energy scales. Each test below specifies an observable, a measurable threshold, and the conditions under which this framework would be challenged.

6.1 Cosmological Synchronization (DESI & Euclid)

In flat ΛCDM, the onset of cosmic acceleration ($q = 0$) and the critical damping of structure growth ($\chi_\delta = 1$) occur at the same transition redshift z_t. Extensions such as curvature or dynamical dark energy ($w(z) \neq -1$) generically break this synchronization, producing an offset $\Delta z = z_{q=0} - z_{\chi=1}$.

- **Observable:** The redshift difference Δz between the kinematic transition ($q = 0$) inferred from supernovae/BAO and the structural transition ($\chi_\delta = 1$) inferred from growth-rate measurements ($f\sigma_8$).

- **Sensitivity Requirement:** Upcoming surveys (DESI, Euclid, Rubin) are expected to constrain $z_t \approx 0.6$ with precision $\sigma_z < 0.05$ [8]. A statistically significant offset $|\Delta z| > 3\sigma_z$ that cannot be attributed to curvature or $w(z)$ evolution would challenge the structural identity.

6.2 Quantum Spectral Merger (Circuit QED)

The transition from underdamped oscillation to overdamped decay at $\chi = 1$ predicts a unique spectral signature: the coalescence of eigenfrequencies into a second-order exceptional point (EP2). This can be probed in superconducting qubit–cavity systems with tunable coupling g [2, 3].

- **Protocol:** A transmon qubit ($\omega_q/2\pi \approx 5$ GHz) coupled to a dissipative cavity ($\kappa/2\pi \approx 1$ MHz) is tuned through the exceptional point by varying the Purcell decay rate $\gamma_P = \kappa g^2/\Delta^2$.

- **Signature:** As χ is scanned through $\{0.8, 0.9, 1.0, 1.1\}$, the qubit population $P_1(t)$ must transition from oscillatory decay $e^{-\gamma t/2}\cos(\omega_a t)$ to the EP2 kernel $te^{-\omega t}$ at the critical point, accompanied by spectral doublet merger $\omega_\pm \to \omega_0$.

- **Sensitivity Requirement:** Time-domain sampling with $\delta t \leq 10$ ns over a $10\,\mu$s window is required to resolve the critical power-law tail. A failure to observe spectral coalescence within the expected window $0.95 < \chi < 1.05$ would challenge the existence of the EP2 boundary in open quantum dynamics. Detailed experimental parameters and statistical hypothesis-testing frameworks are provided in Supplementary Section 9.

6.3 Finite-Temperature QCD Coherence (Lattice)

If the QCD substrate participates in near-critical stability organization, lattice determinations of finite-temperature spectral functions should reveal a scalar (0^{++}) channel with damping ratio $\chi \equiv \Gamma/(2\Omega)$ approaching unity in the vicinity of the confinement transition.

- **Observable:** The thermal pole or peak location $\Omega(T)$ and width $\Gamma(T)$ extracted from spectral reconstructions in the 0^{++} channel.

- **Signature:** Existence of a temperature band near the transition where $0.8 \lesssim \chi(T) \lesssim 1.0$.

- **Challenge condition:** Absence of any near-critical window in all plausible reconstruction methods would weaken the substrate-coherence interpretation.

6.4 Neutron Star Ringdown (Gravitational Waves)

For neutron-star f-modes, the damping time τ and oscillation frequency f define a dimensionless stability index $\chi_{\mathrm{NS}} = (2\pi f\tau)^{-1}$. As compact objects approach the TOV limit, the mode trajectory is predicted to approach the structural boundary $\chi_{\mathrm{NS}} \approx 1$.

- **Test:** Third-generation gravitational-wave detectors (Cosmic Explorer, Einstein Telescope) should observe that remnant objects populate the region $\chi_{\mathrm{NS}} \leq 1$ [5, 21]; a statistically significant population with $\chi_{\mathrm{NS}} > 1$ would contradict the stability-boundary interpretation.

7 Conclusion

A single dimensionless ratio, $\chi = \gamma/(2\omega)$, defines a stability architecture across quantum, field-theoretic, and cosmological dynamics. The critical boundary $\chi = 1$ marks a non-Hermitian exceptional point that coincides exactly with the onset of cosmic acceleration via the identity $\chi_\delta = 1 \iff q = 0$. Substrate inheritance constrains emergent parameters without invoking phenomenological tuning, and observed particle hierarchies are consistent with stability-based classification.

Interpretation. Any apparent preference for $\chi \approx 1$ is interpreted as survivorship under stability constraints rather than as an optimization principle imposed by nature. In this view, the critical boundary functions as a separatrix that organizes which structures can persist, not as a target that dynamics must seek. Together, these results identify χ as a common stability index linking quantum, field-theoretic, and cosmological dissipative dynamics.

Falsifiability. The framework yields several independent tests. (i) In flat ΛCDM, the transitions $\chi_\delta = 1$ and $q = 0$ must coincide; any observed offset would falsify the structural identity. (ii) Finite-temperature lattice QCD must exhibit a 0^{++} mode with $\chi \approx 1$ near the confinement transition. (iii) Quantum platforms with tunable γ/ω must display spectral-peak merger and the EP2 kernel at $\chi = 1$. (iv) Neutron-star oscillation modes should approach $\chi_{\mathrm{NS}} \to 1$ near the TOV limit. These tests collectively determine whether the stability architecture described here is realized in nature.

Methods

Settling-time simulation. Numerical settling times were computed by integrating the second-order damped oscillator

$$\ddot{x} + \gamma \dot{x} + \omega^2 x = 0 \tag{20}$$

via `scipy.integrate.solve_ivp` (Python 3.9+, RK45 adaptive time stepping, absolute and relative tolerances 10^{-9}, maximum step $\Delta t = 0.01$) with unit frequency $\omega = 1$, initial conditions $(x_0, \dot{x}_0) = (1, 0)$, and a damping grid of 120 uniformly spaced values $\chi \in [0.10, 3.0]$, corresponding to $\gamma \in [0.20, 6.0]$. Settling time T_s was defined as the first time at which $|x(t')| \leq 10^{-3}$ for all $t' \geq t$. Results are archived in `symc_settling_times.csv` at Zenodo (`https://doi.org/10.5281/zenodo.17528111`).

Statistical null tests. Cross-scale compression of χ values in Supplementary Table S1 was evaluated against three null models: (N1) permutation of χ relative to mass; (N2) broad log-uniform sampling across the full accessible χ range; (N3) mass-trend-plus-Gaussian-scatter. Each null was evaluated at $n = 10{,}000$ Monte Carlo trials with fixed random seed (seed $= 7$) for reproducibility. Upper-bound entries (electron, proton) were treated as right-censored via log-uniform imputation below the reported limit, repeated over 200 imputations. Primary test statistic was residual standard deviation T_{res} after removing a linear mass trend in log space. Analysis was restricted to the S1 empirical subset ($n = 20$) as the primary result. Source code is archived at Zenodo (`https://doi.org/10.5281/zenodo.17528111`).

Cosmological calculations. The identity $\chi_\delta = 1 \iff q = 0$ was derived analytically from the flat-ΛCDM Friedmann and growth equations (Section 3 and Supplementary Section 1.3). Figure 2(a) plots $q(z)$ and $\chi_\delta(z)$ computed directly from these equations; no fitting functions are used. Numerical verification used concordance parameters $\Omega_m = 0.315$, $\Omega_\Lambda = 0.685$, $H_0 = 67.4$ km s^{-1} Mpc^{-1} [19]. Sensitivity of the synchronization redshift to wCDM departures was computed over a grid of (w_0, w_a) values; results are tabulated in `phase1_deltaa_grid.csv` and `phase1_validity_table.csv`, provided in the Supplementary Materials.

Particle data compilation. Mass and width values in Supplementary Table S1 were drawn from PDG 2022 [16]. Vacuum-scale entries (QCD, Electroweak, GUT, Planck, Dark Energy) are defined anchors satisfying $\chi = 1$ by construction ($\Gamma = 2\omega$) and are plotted as open markers in Figure 3 to distinguish them from empirical data; they are excluded from statistical compression estimates.

Quark widths represent the hadronization scale $\sim \Lambda_{\mathrm{QCD}}$ and are approximate. Electron and proton widths are PDG-derived experimental upper bounds. Neutrino entries report mass scales only; coherence constraints imply $\chi_k \ll 1$ without a specific Γ. Figure 3 is generated from a canonical data file (`stability_table_S1.csv`) using a reproducible Python script (`figure3_clean.py`); both are archived at Zenodo (`https://doi.org/10.5281/zenodo.17528111`). Full conventions and provenance are given in Supplementary Table S1.

Author Contributions

N.C. conceived the theoretical framework, performed the derivations, conducted the analysis, and prepared the manuscript and supplementary materials.

Competing Interests

The author declares no competing interests.

Data availability

The settling-time simulation data supporting this study (`symc_settling_times.csv`), cosmological sensitivity grids (`phase1_deltaa_grid.csv`, `phase1_validity_table.csv`), canonical particle data file (`stability_table_S1.csv`), and complete source code (`figure3_clean.py`, `chi_null_tests.py`) are available at Zenodo (`https://doi.org/10.5281/zenodo.17528111`) and GitHub (`https://github.com/SymCUniverse/Foundations`). All particle physics values are drawn from PDG 2022 [16].

AI Writing Assistance

During the preparation of this work, the author used Claude (Anthropic), GPT-4 (OpenAI), DeepSeek, Gemini (Google), and Microsoft Copilot in a systematic convergence methodology to cross-check mathematical derivations, test theoretical claims, and refine hypothesis formulation through iterative dialogue. Multiple AI systems were queried independently on identical problems to identify consensus solutions and flag inconsistencies requiring further investigation. The author orchestrated all queries, evaluated all outputs critically, and edited all content for accuracy and clarity. All data analysis, scientific conclusions, theoretical framework development, and final manuscript content are the original intellectual contribution of the author. The author takes full responsibility for the accuracy and integrity of this work.

References

[1] Bender, C. M. Making sense of non-Hermitian Hamiltonians. *Rep. Prog. Phys.* **70**, 947–1018 (2007).

[2] Aspelmeyer, M., Kippenberg, T. J. & Marquardt, F. Cavity optomechanics. *Rev. Mod. Phys.* **86**, 1391–1452 (2014).

[3] Blais, A. et al. Circuit quantum electrodynamics. *Rev. Mod. Phys.* **93**, 025005 (2021).

[4] Breuer, H.-P. & Petruccione, F. *The Theory of Open Quantum Systems* (Oxford University Press, 2002).

[5] Cardoso, V., Franzin, E. & Pani, P. Is the gravitational-wave ringdown a probe of the event horizon? *Phys. Rev. Lett.* **116**, 171101 (2016).

[6] Carmichael, H. J. *Statistical Methods in Quantum Optics 1* (Springer, 1999).

[7] Clerk, A. A. et al. Introduction to quantum noise, measurement, and amplification. *Rev. Mod. Phys.* **82**, 1155–1208 (2010).

[8] DESI Collaboration. DESI 2024 VI: cosmological constraints from BAO. Preprint at `https://arxiv.org/abs/2404.03002` (2024).

[9] Dodelson, S. *Modern Cosmology* (Academic Press, 2003).

[10] Gorini, V., Kossakowski, A. & Sudarshan, E. C. G. Completely positive dynamical semigroups of N-level systems. *J. Math. Phys.* **17**, 821–825 (1976).

[11] Heiss, W. D. The physics of exceptional points. *J. Phys. A* **45**, 444016 (2012).

[12] Kato, T. *Perturbation Theory for Linear Operators* (Springer, 1995).

[13] Bergholtz, E. J., Budich, J. C. & Kunst, F. K. Exceptional topology of non-Hermitian systems. *Rev. Mod. Phys.* **93**, 015005 (2021).

[14] Lindblad, G. On the generators of quantum dynamical semigroups. *Commun. Math. Phys.* **48**, 119–130 (1976).

[15] Ogata, K. *Modern Control Engineering* 5th edn (Prentice Hall, 2010).

[16] Particle Data Group. Review of particle physics. *Prog. Theor. Exp. Phys.* **2022**, 083C01 (2022).

[17] Peebles, P. J. E. *Principles of Physical Cosmology* (Princeton University Press, 1993).

[18] Perlmutter, S. et al. Measurements of Ω and Λ from 42 high-redshift supernovae. *Astrophys. J.* **517**, 565–586 (1999).

[19] Planck Collaboration. Planck 2018 results. VI. Cosmological parameters. *Astron. Astrophys.* **641**, A6 (2020).

[20] Riess, A. G. et al. Observational evidence from supernovae for an accelerating universe. *Astron. J.* **116**, 1009–1038 (1998).

[21] Abbott, B. P. et al. GW190814: gravitational waves from the coalescence of a 23 solar mass black hole with a 2.6 solar mass compact object. *Astrophys. J. Lett.* **896**, L44 (2020).

[22] Wilson, K. G. & Kogut, J. The renormalization group and the ϵ expansion. *Phys. Rep.* **12**, 75–199 (1974).

[23] Christensen, N. Structural constraints from critical damping in open quantum field theories: implications for QCD substrate inheritance and phenomenological extensions. Zenodo `https://doi.org/10.5281/zenodo.17437688` (2026).

[24] Christensen, N. Closing critical gaps: physical inheritance from stabilized substrates in dynamical systems. Zenodo `https://doi.org/10.5281/zenodo.17428940` (2026).